Impact of Late Universe Constraints on Early Universe Measurements of Hubble

Garrett Suggs

A senior thesis submitted to the faculty of
Brigham Young University
in partial fulfillment of the requirements for the degree of

Bachelor of Science

Christopher B. Verhaaren, Advisor

Department of Physics and Astronomy

Brigham Young University

ABSTRACT

Impact of Late Universe Constraints on Early Universe Measurements of Hubble

Garrett Suggs
Department of Physics and Astronomy, BYU
Bachelor of Science

Early universe measurements of the Hubble constant usually find the best-fit value for H_0 given a specific data set and a particular cosmological model. Planck's all-sky survey of the Cosmic Microwave Background is a common choice for this data, and is often supplemented with additional constraints from other measurements of cosmological phenomena. For example, the SH0ES collaboration's measurement of H_0 from local type Ia supernovae is a common constraint to include, in the hope of reconciling the tension between late and early universe measurements. We attempt to quantify the effect of this constraint on early universe measurements of H_0. We obtain values for H_0 from several cosmological models—ΛCDM, CPL dark energy, and exponential acoustic dark energy—under two sets of constraints: only CMB data, and CMB data as well as the SH0ES measurement. We compare these results to each other and find that, for these models, constraining the H_0 measurement with SH0ES' measurement generally reduces the Hubble tension by $\sim 0.5\sigma$. Given the limited scope of this study, our results are probably not generalizable to models other than the ones we examined.

Keywords: cosmology, Hubble, SH0ES, Planck

ACKNOWLEDGMENTS

Many thanks to Rubén Arjona, Steven Clark, William Black, and Nikolai Wallin for providing significant assistance with the various pieces of software I have used in this thesis.

I would also like to express my gratitude to my advisor, Dr. Chris Verhaaren, and to Dr. Karine Chesnel and Dr. Benjamin Boizelle for serving on my thesis committee. Their feedback and support has greatly elevated the quality of this thesis.

Thanks as well to the BYU Office of Research Computing for providing computational resources, as well as frequent assistance with troubleshooting.

I also thank the BYU College of Computational, Mathematical, and Physical sciences for providing the funding that enabled me to invest myself so deeply in this project.

Based on observations obtained with Planck (http://www.esa.int/Planck), an ESA science mission with instruments and contributions directly funded by ESA Member States, NASA, and Canada.

Contents

List of Figures

List of Tables

Chapter 1

Introduction

The primary goal of cosmology is to describe the origins, present state, and eventual fate of the universe. For something like a star, we might approach this by asking questions about its properties: how much mass does it have? How large is its radius? How hot is it? Similarly, the universe has some macro-scale properties that we can describe that help us understand its evolution.

One such property is its current expansion rate, called the Hubble constant. The universe's expansion was first predicted theoretically in the early 1920s by Alexander Friedmann [1]. Cosmology uses the quantity a, called the scale factor, to describe the size of the universe. The present scale factor is $a_0 = 1$, and as we go further back in time, $a \to 0$. Friedmann showed that the scale factor evolves according to

$$\left(\frac{\dot{a}}{a}\right)^2 = \frac{8\pi G}{3c^2}\rho(t) - \frac{\kappa c^2}{R_0^2 a^2} + \frac{\Lambda}{3} \tag{1.1}$$

in a homogeneous and isotropic universe, with spatially uniform density. Here, G is the gravitational constant, c is the speed of light, ρ is the energy density of the universe, κ encodes the direction of the universe's curvature (closed, open, or flat), and R_0 is the radius of curvature [2].

The Λ term did not appear in Friedmann's original derivation; it was added later to account for the possibility of the expansion accelerating positively and is related to the energy density of dark

energy [2]. Dark energy is a cosmological component with negative pressure, thus encouraging the expansion of the universe rather than its collapse like "normal" matter and energy do. This negative pressure is usually described by way of an equation of state:

$$w = \frac{P}{\rho}, \tag{1.2}$$

where P is the pressure due to some cosmological component, ρ is the energy density of said component, and w is equivalently called the equation of state or the equation of state parameter [2]. Since a negative density would be unphysical, w being negative implies a negative pressure. As Λ is usually thought of as being constant, w_Λ is also a constant -1 [2].

The Friedmann equation does not explicitly require expansion, but it certainly allows it. Observational evidence for expansion came a bit later, most notably from Edwin Hubble (for whom the Hubble constant is named) in 1929 [3]. Since then, the Hubble constant—which is just the present value of the Hubble parameter $H(t) \equiv \dot{a}/a$, and usually denoted H_0—has been measured many times with increasing accuracy. Ref. [4] summarizes many of these measurements, and the recent history of measurements is illustrated graphically in figure 1.1. Recent evidence strongly indicates that the expansion rate is positively accelerating, [5] so dark energy has become an important feature of modern cosmological models, often taking the form of the constant dark energy described by Λ.

There are many techniques for measuring H_0, but every measurement can be broadly categorized as a "late universe" or "early universe" measurement [4]. Late measurements are based on data from $a \sim 1$, like measurements of galaxies' distances and recessional velocities; and early measurements are based on data from $a \lesssim 0.001$, like the cosmic microwave background (CMB) [4]. Historically these types of measurements were in agreement with each other due to their relatively large uncertainties; however, with the arrival of data from the Planck satellite in 2013, a tension started to grow, as seen in figure 1.2. The Planck collaboration—using all-sky CMB data from the Planck satellite—finds $H_0 = 67.4 \pm 0.5$ km s^{-1} Mpc^{-1} [7]. In contrast, the most precise late measurement comes primarily from Hubble Space Telescope data by way of the SH0ES (Supernova H_0 for the

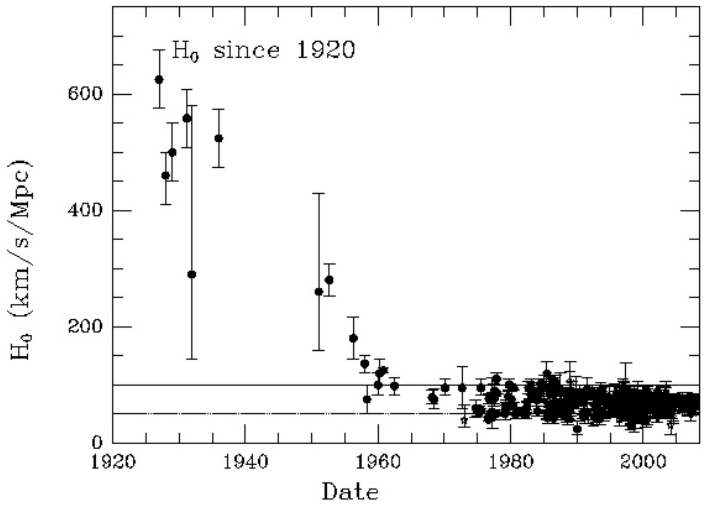

Figure 1.1 H_0 measurements since the early 1900s. The first measurement actually comes from Georges Lemaître, who published a value for H_0 based on Hubble's data before Hubble himself did. From ref. [6]

.

Equation of State) collaboration, and gives $H_0 = 73.04 \pm 1.04$ km s^{-1} Mpc^{-1} [8].

To compute the magnitude of this tension, we treat each measurement as a normal distribution, with the standard deviations given by their respective uncertainties. We then consider the distribution of differences between measurements. The mean of such a distribution is given by the difference of the means, and the standard deviation is given by the square root of the sum of the squares of the uncertainties. Mathematically, we represent this as

$$N_1(m_1, \sigma_1) - N_2(m_2, \sigma_2) = N_3\left(m_1 - m_2, \sqrt{\sigma_1^2 + \sigma_2^2}\right). \tag{1.3}$$

Here, $N_{1,2}$ represent the distributions of the respective measurements, N_3 is the distribution of differences, and m_i and σ_i are the uncertainties. This means we can compute a disagreement of $n\sigma$ as

$$n\sigma = \frac{|m_1 - m_2|}{\sqrt{\sigma_1^2 + \sigma_2^2}}\sigma, \tag{1.4}$$

and we can interpret the result as telling us the difference between measurements 1 and 2 is n

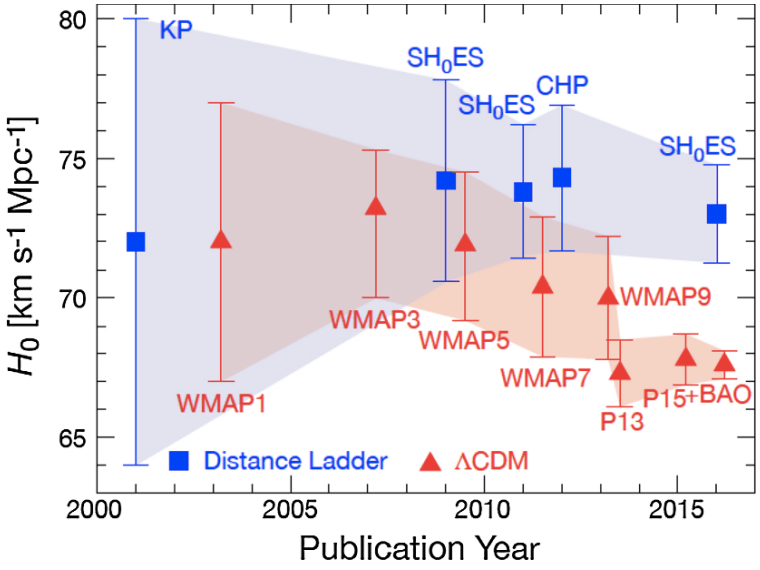

Figure 1.2 H_0 measurements since 2000, showing the growing tension. Not all measurements are illustrated here of course—these are just the most precise ones. Note that while there is definitely a tension by the time of the first Planck measurement (P13), there was already some discrepancy by the last few WMAP (Wilkinson Microwave Anisotropy Probe, Planck's predecessor) measurements. From ref. [9].

standard deviations away from zero [10]. When we compute the tension between the Planck and SH0ES measurements of H_0, we find they disagree by approximately 5σ. This disagreement is known as the Hubble tension, and is one of the most significant problems in modern cosmology, as evidenced by the more than 300 publications on the subject posted to arXiv since December 2023.

One of the main interpretations of the Hubble tension is that the Planck value for H_0 is too low—that it should be more similar to the SH0ES value. There is ample reason to believe this: the Planck collaboration's methods are highly sensitive to the underlying physics, so choosing a different cosmological model can change predicted parameter values fairly easily. The parameter values published by Planck are based on the standard cosmological model, called ΛCDM. This model derives its name from the Λ term in equation 1.1, as it uses dark energy with $w = -1$, and cold dark matter (CDM). Proposed solutions to the Hubble tension often take the form of modifications to one of these components. These modifications can be quite varied in nature and include giving dark

energy time-varying behavior or adding self-interacting dark matter components. Solutions also occasionally introduce modifications to other components of ΛCDM, like modified gravitational models instead of general relativity. Ref. [4] reviews some of these modifications, and finds that models which can alleviate the Hubble tension include time dependent dark energy models (where w is not constant), as well as some modified gravities. Testing these modified cosmologies gives us a fantastic way to probe new fundamental physics: if they predict an H_0 value in better agreement with the SH0ES value, they may be good candidates to replace ΛCDM.

We can obtain a prediction for H_0 from each of these modified cosmologies by using the same methods the Planck collaboration employed. There are three primary elements to Planck's approach: a cosmological theory code, a "likelihood" from some data (such as the CMB) which puts constraints on allowed values for certain parameters, and a Markov Chain Monte Carlo (MCMC) sampler [11]. Besides the Planck CMB data, further constraints from other datasets can be imposed by utilizing other likelihoods. One common choice is using the SH0ES measurement as a simple Gaussian prior constraint on H_0. We might hope that this will bring the predicted value of H_0 closer to the SH0ES value and speed up runtimes since the allowed portion of the parameter space will be smaller. Further, H_0 may be poorly constrained by the CMB alone in the context of some chosen cosmology, so adding extra constraints could lead to tighter uncertainties. However, one might naively expect that if a new cosmological model were to resolve the Hubble tension, it would be able to do so with no additional constraints beyond the CMB.

This work attempts to address this last point. We aim to examine the impact of using this likelihood from SH0ES when optimizing modified cosmologies and elucidate why it may be useful. Our framework for this will be to do MCMC runs on a variety of cosmological models, both with and without the SH0ES constraint. We will compare the H_0 predictions from each of these runs and try to identify any patterns that may present themselves. Besides Planck likelihoods to encode the CMB data, we restrict ourselves to using the SH0ES likelihood so we can try to isolate its

impact on an H_0 measurement. We will do base ΛCDM runs for the purpose of comparison. All of the modified models we will use will be dynamical dark energy models for simplicity. These have a time-varying equation of state for the dark energy component, as opposed to ΛCDM's constant equation of state. In particular, we will focus on Chevallier-Polarski-Linder (CPL) dark energy [12, 13] and so-called exponential acoustic dark energy (EADE) [14], as they are fairly mathematically simple and therefore easier to get started with.

In the next chapter, we will discuss our methods in greater detail, focusing on the process used to go from CMB data and a cosmological model to a measurement of H_0. We will also discuss some details of the implementation of cosmological models into computer code. In the final chapter, we will discuss our results. While we will not discuss the details of the SH0ES measurement of H_0 further in the main body of this paper, it is valuable information, so the interested reader can find a brief overview in appendix A. Similarly, additional background information on the Planck measurement of H_0 can be found in appendix B.

Chapter 2

MCMC analysis of dynamical dark energy models

In order to examine the use of the SH0ES likelihood, we will focus on early universe measurements of H_0 from the CMB. We defer a more detailed explanation of the CMB's formation to appendix B; here, we merely note that the CMB formed during a period known as recombination. The CMB has an average temperature of about 2.7255 K [2]. While this temperature is very close to uniform, it is not entirely so. It has random deviations on the scale of a few hundred μK; these can be seen in figure 2.1, which is the Planck collaboration's all-sky temperature map of the CMB.

We can mathematically define these deviations from the average temperature as

$$\frac{\delta T}{T}(\theta,\phi) = \frac{T(\theta,\phi) - \langle T \rangle}{\langle T \rangle}, \tag{2.1}$$

where $\langle T \rangle$ is the average temperature and $T(\theta,\phi)$ gives the temperature at some arbitrary position on the sky. Note that this quantity is dimensionless. It is convenient to express these deviations as an expansion in spherical harmonics:

$$\frac{\delta T}{T}(\theta,\phi) = \sum_{l=0}^{\infty} \sum_{m=-l}^{l} a_{lm} Y_{lm}(\theta,\phi). \tag{2.2}$$

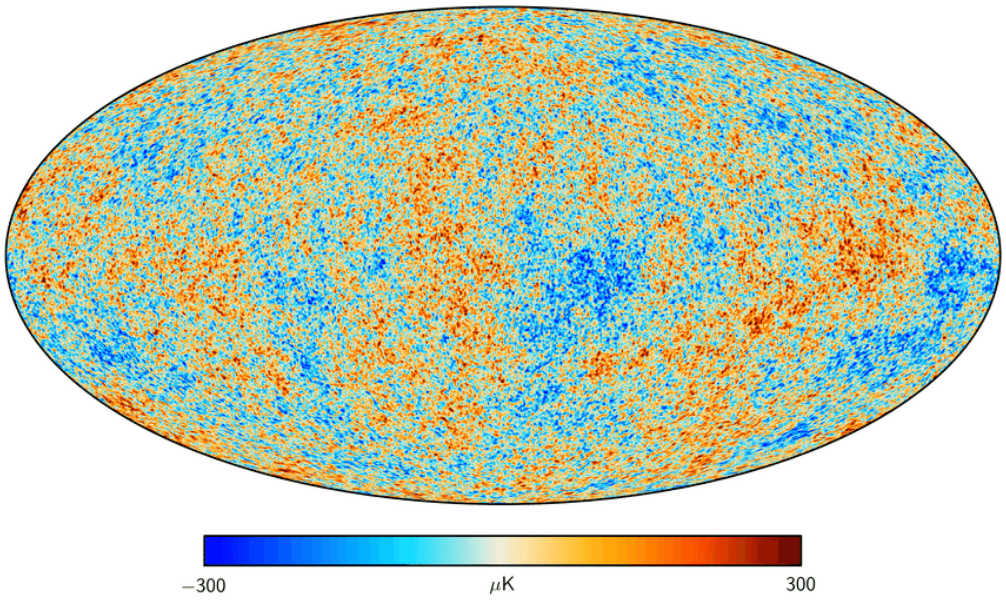

Figure 2.1 All-sky temperature map of the CMB, from the Planck collaboration [15]. The average temperature has been subtracted off, so that we are only looking at the deviations. Blue spots are colder, red spots are warmer. The maximum deviation is 300 μK.

Here, $\delta T/T$ is the same quantity defined above, and $Y_{lm}(\theta,\phi) \propto P_{lm}(\cos\theta)e^{im\phi}$ are the spherical harmonic functions with the P_{lm} being the associated Legendre polynomials. The number l is called the "multipole", and encodes an angular scale—larger l means a smaller angular scale [2].

From here, we can compute the two-point correlation function $C(\theta)$, which describes how similar the temperatures at points separated by angle θ are. This is given by

$$C(\theta) = \left\langle \frac{\delta T}{T}(\hat{n}) \frac{\delta T}{T}(\hat{n}') \right\rangle_{\hat{n}\cdot\hat{n}'=\cos\theta}. \tag{2.3}$$

Here, $\hat{n}$ and $\hat{n}'$ give the directions to two separate temperature fluctuations. We are taking the product of these two fluctuations, and averaging over all points separated by angle θ [2]. With the temperature deviations in spherical harmonics, the correlation function is usually expressed as

$$C(\theta) = \frac{1}{4\pi}\sum_{l=0}^{\infty}(2l+1)C_l P_l(\cos\theta), \tag{2.4}$$

where the P_l are the Legendre polynomials and are related to the associated Legendre polynomials as $P_{l,m=0} = P_l$ [2]. The coefficients C_l, often scaled by some convenient factor, are known as the

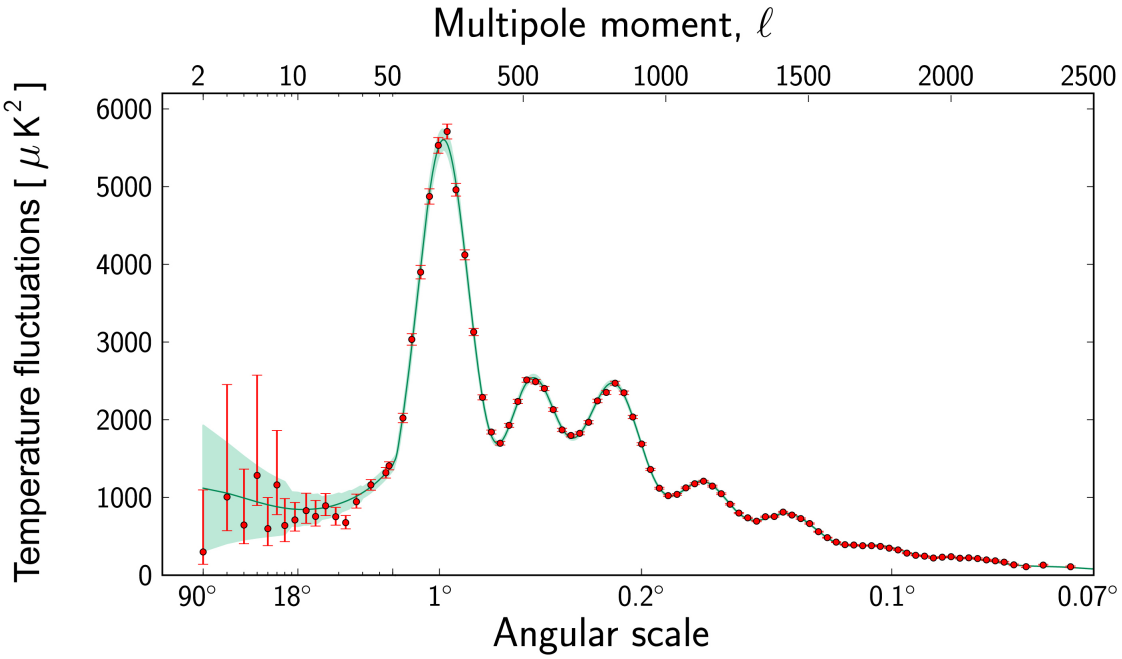

Figure 2.2 The power spectrum of CMB temperature fluctuations as measured by the Planck satellite—roughly, the magnitude of the deviation from average as a function of angular scale. Note that the fluctuations are roughly constant up to about 10°, at which point we enter a series of peaks and valleys. The shapes of these peaks and the overall shape of the spectrum are correlated with various cosmological parameters, which is what enables us to derive parameter values from the CMB. From ref. [16].

temperature power spectrum of the CMB and are proportional to the average over m of a_{lm}^2, as we can see from equation 2.3. This power spectrum is plotted in figure 2.2.

Additional power spectra can be generated by considering the amount of CMB light that is polarized [4]. These power spectra also provide constraints on cosmological parameters, and are defined similarly to the temperature power spectrum except that they only consider polarized light.

The CMB was first detected in 1964 by Arno Penzias and Robert Wilson, using a ground-based radio antenna [2]. One of the earliest measurements of its temperature power spectrum came with the launch of the COBE satellite in 1989; [17] COBE was followed by the WMAP satellite in the

early 2000s [2] and the Planck satellite in the early 2010s [18]. We will make use of Planck's data, as it is the most precise all-sky data to date, and its use is standard in the type of analysis we will conduct. This analysis can be thought of simply as fitting a model to some data—the model being ΛCDM or some other cosmological model, and the data being the CMB power spectrum. The typical parameters used in the fit for ΛCDM are $\Omega_b h^2$, $\Omega_c h^2$, $100\theta_s$, τ, n_s, and $\ln\left(10^{10}A_s\right)$ [7]. We explain $100\theta_s$ in more detail in appendix B; the other parameters are less important to measuring H_0 so we will only give them brief attention there. For now, we only state their names and observe that $100\theta_s$ is a good probe for the value of H_0.

We primarily follow the methodology established in [11] to derive values for H_0 from a variety of cosmological models. This process relies on three computational components: a cosmological theory code such as `CLASS` [19], an MCMC sampler—in our case, `Cobaya` [20,21]—to test a variety of values for the fit parameters, and one or more likelihoods (bundled with `Cobaya`) to constrain parameter values. `Cobaya` picks a set of values for the fit parameters and passes those to `CLASS`, which computes the CMB temperature power spectrum from them. `CLASS` passes this computed spectrum back to `Cobaya`, which compares it with the actual power spectrum measured by the Planck satellite using the likelihood(s). This process usually runs several times in parallel. Over thousands of iterations, a posterior probability distribution for each input parameter is created. The simulation runs until a chosen convergence criterion is reached. Our chosen criterion is $R-1$, which measures how similar the mean values for each of the parallel runs are. Lower values are better, so we set the runs to terminate when $R-1<0.01$. The mean value of a given posterior distribution is then taken as the prediction for that parameter. We have illustrated this process schematically in figure 2.3.

We should note that there are several algorithms we could use within the theory code. `CLASS` offers `HyRec` and `RECFAST` as two options for computing recombination processes, and `HALOFIT` and `HMcode` for computing matter distribution. `HyRec` assumes a dark energy equation of state of

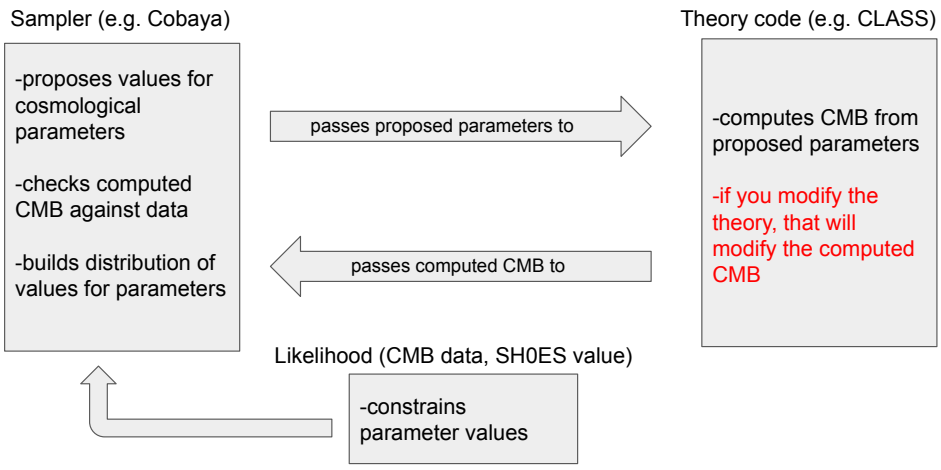

Figure 2.3 Schematic illustration of the computational process for finding cosmological parameter values. For each computational component, we have listed some examples of software/data that could be used in that role.

the form of equation 2.6, while `RECFAST` is more generic. As the dark energy equation of state for one of our models is significantly different from equation 2.6, we use `RECFAST` for that model and `HyRec` for the other two. We have also chosen to use `HALOFIT`, as we had trouble getting `HMcode` to parallelize correctly.

As noted earlier, we can use likelihood distributions from a variety of sources to constrain the fit parameters. The minimal case is to use only Planck likelihoods; this includes likelihoods for the temperature power spectrum, as well as for the polarization power spectra. These likelihoods can constrain the standard six fit parameters well. Further, we could incorporate likelihoods from any number of other sources. Common choices include Baryon Acoustic Oscillations, Type Ia supernovae surveys, and the SH0ES measurement of H_0 [4]. Each likelihood will constrain something different; in particular, the SH0ES likelihood only directly constrains H_0. Our goal is to examine the impact of this constraint from SH0ES on measured values of H_0.

We will analyze three models twice each: ΛCDM as a baseline, CPL dark energy, [12, 13] and exponential acoustic dark energy (EADE) [14]. We will conduct MCMC runs on each model both with and without the SH0ES constraint, and compare the results to see if we can identify any patterns. We will discuss each model individually.

2.1 ΛCDM

We give more background on ΛCDM in appendix B, but it has several defining features we will discuss briefly here. First, dark energy is modeled as a cosmological constant. This is the Λ in the model's name. By cosmological constant, we mean that its energy density does not dilute as the universe expands, like one might expect for something like matter. This is mathematically modeled by setting its equation of state to a constant; in this case,

$$w(a) = -1, \tag{2.5}$$

where a is the cosmological scale factor (often used as a proxy for cosmic time). Second, dark matter is modeled as cold dark matter (the CDM in the name). Cold dark matter only interacts with itself and normal matter gravitationally, and is not relativistic. (This latter criterion must be true; else structures smaller than galactic clusters would have difficulty forming and would be newer in the universe's evolutionary history than they actually are [2].) Finally, we use general relativity as the gravitational model [18].

H_0 has been measured from the CMB using ΛCDM many times, most notably in our case by the Planck collaboration [7]. Consequently, this particular part of the analysis did not require much effort: `Cobaya` comes with a very useful input file generator that gives reasonable initial values for the standard six fit parameters, and can incorporate the SH0ES constraint. Thus, for our analysis, we used this input generator to create input files for base ΛCDM and ΛCDM+SH0ES runs [22–26]. The MCMC runs were performed on BYU's Mary Lou Fulton supercomputer, and we generated

corner plots of the posterior distributions using `GetDist`, [27] a Python package built for such purposes.

2.2 CPL dark energy

Chevallier-Polarski-Linder (CPL) dark energy [12, 13] is a simple dynamical dark energy model. It differs from ΛCDM in only one respect, which is that it replaces the constant dark energy equation of state with

$$w(a) = w_0 + w_a(1-a). \tag{2.6}$$

In this equation, w_0 is the current value of $w(a)$, and w_a defines the evolution of w with a. These two parameters, in addition to the six mentioned earlier, are the fit parameters for this model. The equation of state is plotted in figure 2.4. This model is also sometimes known as the w_0w_aCDM model.

CPL dark energy is already implemented in the current version of `CLASS`, where it is modeled as a fluid. CPL dark energy is also well supported by `Cobaya`, where it is one of the model options in the input file generator. Thus, we were once again able to simply have `Cobaya` generate the initial values and start the runs [22–26]. The only minor complication arose from the fact that when we ran the code on the supercomputer, it would consistently fail to find a feasible initial point for the sampling process, and thus fail to run. We are unsure what caused this issue: the same input file worked with no issues on a personal computer. Thus, we conducted the CPL runs on said personal computer, though we note that this could in theory make our results less comparable with each other. Plots were again generated using `GetDist`.

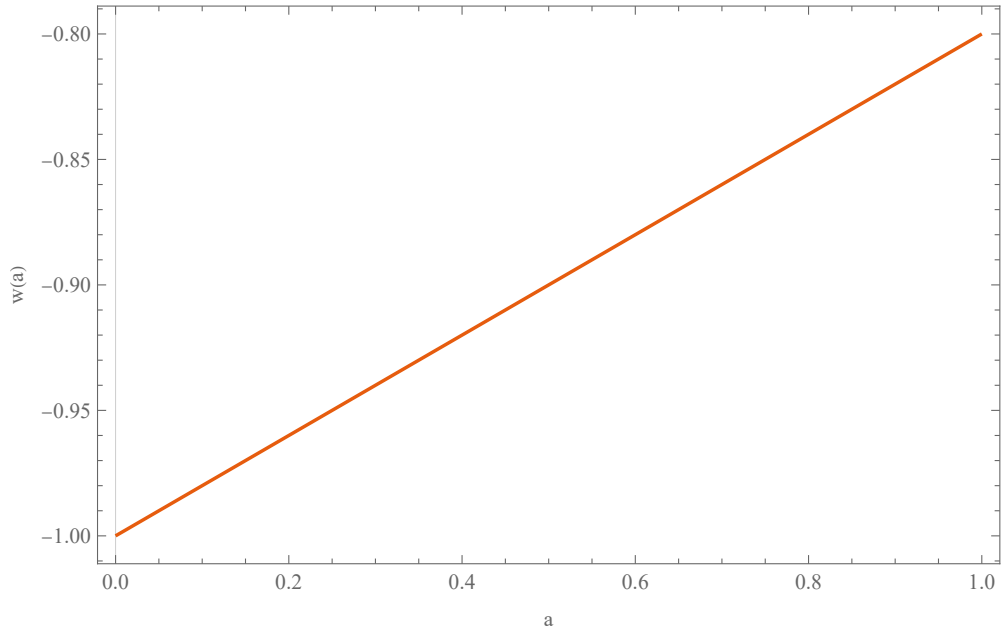

Figure 2.4 The equation of state for CPL dark energy as a function of scale factor (eq. 2.6). Here we have set $w_0 = -0.8$ and $w_a = -0.2$; however, it should be clear that changing the values of these parameters does not change the general shape of this evolution at all.

2.3 EADE

The final model we will consider is called exponential acoustic dark energy (EADE) [14]. This model is, in many respects, very similar to CPL dark energy, in that all it changes from ΛCDM is the dark energy equation of state. It differs slightly from CPL both in the exact form of the equation of state, and in that we only apply this new equation of state to a fraction of the total dark energy. The new equation of state is

$$w(a) = 2^{\left(1-\frac{a_c}{2a}\right)} - 1. \tag{2.7}$$

Here, a_c is a critical scale factor which controls a transition in the behavior of the dark energy, and is one of the fit parameters for the model. This equation of state is plotted in figure 2.5. Note that as $a \to 0$, $w \to -1$.

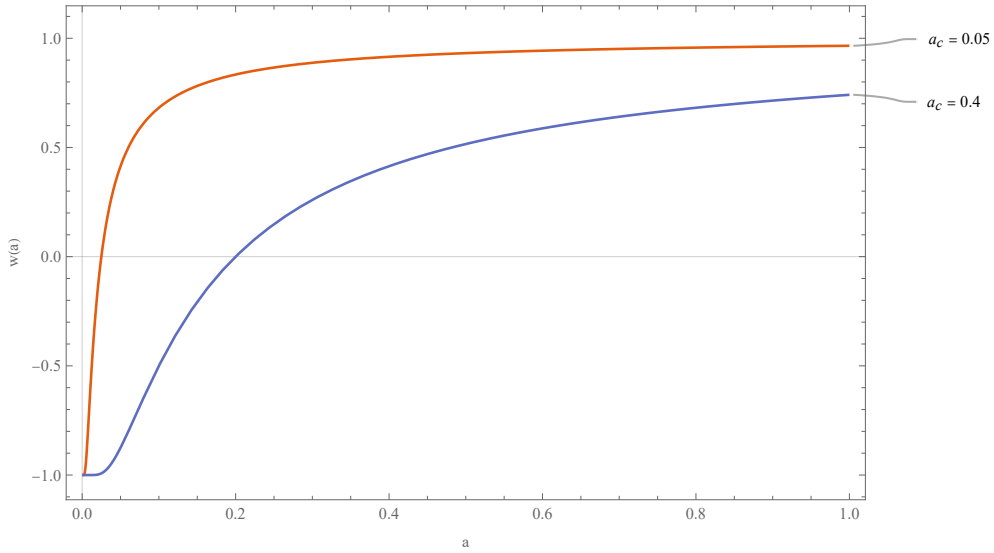

Figure 2.5 The equation of state for exponential acoustic dark energy as a function of scale factor (eq. 2.7). The red line is $w(a)$ with $a_c = 0.05$, while the blue line has $a_c = 0.4$. As can be seen, increasing a_c shifts the epoch of transition towards the present, and makes the transition happen more slowly. If a_c is sufficiently small, the transition happens quickly; as a_c increases the curve becomes more sigmoid in shape.

The other fit parameter we use is the density fraction of this component of dark energy:

$$\Omega_{0,\mathrm{EADE}} \equiv \frac{\rho_{0,\mathrm{EADE}}}{\rho_{c,0}}, \tag{2.8}$$

where $\rho_{c,0} = \frac{3H_0^2}{8\pi G}$ is the critical density at present and the subscript 0 denotes the value of a parameter at the present time. This differs slightly from the second fit parameter in the original paper, which uses

$$f_c \equiv \frac{\rho_{\mathrm{EADE}}(a_c)}{\rho_{tot}(a_c)}. \tag{2.9}$$

This difference stems from a difference in theory codes: we are using `CLASS`, while the original paper used a code called `CAMB` [28, 29]. These codes are extremely similar: they both seek to compute the same things, and share many subroutines. (For instance, both rely on codes like `RECFAST` to handle certain computations.) However, at least for models like EADE, `CAMB` uses the f_c parameter instead of an Ω_0 parameter. As far as we know, there is no explicit advantage to one or

the other; they are merely two ways of looking at the same problem, and should give similar results. That being said, this difference in implementation slightly limits our ability to compare our results to the original paper [14].

We should note that ref. [14] does provide an equation to convert from f_c to Ω:

$$\Omega_{EADE}(a) = 2f_c \frac{(c_s^2+1)^2 - (w_{EADE}(a)+1)^2}{(c_s^2+1)^2}. \tag{2.10}$$

However, when we used this equation in `CLASS` and attempted to sample—using the best-fit values from [14] to inform the initial point—`Cobaya` could not find any feasible points. Passing the best fit parameters directly to `CLASS`—that is, computing a single point instead of the entire distribution—produced a value for the Hubble constant of $H_0 \sim 20$ km s^{-1} Mpc^{-1}, in contrast to ref. [14]'s reported value of ~ 70 km s^{-1} Mpc^{-1}. As we were unable to determine the cause of the discrepancy, we have settled for using Ω_{EADE} instead of f_c. We will still use equation (2.10) to compare our results to the original results, but because this equation was not able to produce similar results in the first place, we are somewhat doubtful as to its applicability.

These nuances aside, this model is straightforward to implement into `CLASS` : the model can be approximated as a perfect fluid, and `CLASS` already supports such models. Thus, creating an EADE-capable version of `CLASS` is as simple as locating all of the sections of code that deal with fluid dark energy and adding an extra logic check and appropriate equations to handle EADE. We also changed the default recombination code from `HyRec` to `RECFAST`, as `HyRec` assumes that the dark energy equation of state roughly follows the form of equation 2.6, which is incompatible with EADE's equation of state.

The only nontrivial step of implementation required the use of the GNU Scientific Library to compute the numeric integral

$$\rho_{\mathrm{EADE}}(a_{\mathrm{ini}}) = \rho_{0,\mathrm{EADE}} \exp\left(\int_{a_{\mathrm{ini}}}^{a_0} da\, 3\, \frac{1+w_{EADE}(a)}{a}\right). \tag{2.11}$$

Here, a_{ini} is `CLASS`' approximation to the scale factor at the beginning of the universe. Strictly,

this should be $a = 0$, but because of finite precision considerations, is actually $a \ll 1$. Thus, this equation computes the energy density of EADE at very early times, based on the density at the present.

We used the same maximum range for a_c as ref. [14] did, and we based the shape of the prior distribution on their best-fit value for a_c. We loosely based our initial distribution for Ω_{EADE} on the best-fit value for f_c, which produced a small Ω_{EADE} by way of equation 2.10. The MCMC runs for EADE were performed on BYU's supercomputer, and plots were generated with `GetDist`.

Chapter 3

Results

We now turn our attention to the actual values for H_0 we obtained from our analysis. We will spend some time discussing the results for each model in more particular detail, but our results are summarized in table 3.1. We also summarize the tension between each of these measurements and the SH0ES measurement in the same table; as can be seen, the SH0ES constraint consistently reduced the tension, though not necessarily by a very significant amount.

3.1 ΛCDM

Our ΛCDM value, when constrained only by the CMB, is $H_0 = 67.20 \pm 0.48$ km s^{-1} Mpc^{-1}. This closely matches the value obtained by the Planck collaboration (67.4 ± 0.5 km s^{-1} Mpc^{-1}), and provides a good baseline for verifying that we have `CLASS` and `Cobaya` functioning properly. When we constrain ΛCDM additionally with SH0ES, the H_0 value is closer to the SH0ES value, as expected. However, the difference is not particularly large—only about 0.8 km s^{-1} Mpc^{-1}, for a total change in tension of 0.64σ.

A corner plot for the six fit parameters (plus H_0), showing both runs, can be found in figure 3.1. With only a couple of exceptions, the distributions are noticeably different between runs; most

Model	Constraints	H_0	Tension with SH0ES	χ^2	R − 1
———	SH0ES	73.04 ± 1.04	————	—	——
ΛCDM	CMB	67.20 ± 0.48	5.10σ	10984.2	0.008865
	CMB+SH0ES	67.97 ± 0.46	4.46σ	11003.2	0.009309
CPL	CMB	90.92 ± 17.99	0.99σ	10983.3	0.009372
	CMB+SH0ES	73.27 ± 1.31	0.14σ	10984	0.009936
EADE	CMB	66.27 ± 0.95	4.81σ	10985.6	0.009029
	CMB+SH0ES	67.78 ± 0.50	4.56σ	11004.6	0.006816

Table 3.1 H_0 predictions and statistical tensions with the SH0ES measurement ($H_0 = 73.04 \pm 1.04$ km s^{-1} Mpc^{-1} [8]) for each cosmological model and constraint combination. The CMB constraints come from Planck; CMB+SH0ES combines that data with the SH0ES distance ladder measurement of H_0. All H_0 values are reported in the standard units of km s^{-1} Mpc^{-1}, and the given uncertainties are the 68% confidence level intervals from the fit. The tensions are computed as described in equation 1.4. Additionally, we report goodness-of-fit as determined by the χ^2 statistic for each run—lower values are better, so for our results CPL is the best fit to the data. Finally, we report the $R-1$ convergence statistic for each run; this is essentially a measure of whether the MCMC algorithm is done. Values closer to zero are better. We set each run to finish when $R-1$ became less than 0.1. Initial $R-1$ values are typically about 10, so these runs are well converged.

importantly, H_0 is consistently shifted to higher values.

3.2 CPL dark energy

H_0 is poorly constrained by only CMB data in the CPL model: we found $H_0 = 90.92 \pm 17.99$ km s^{-1} Mpc^{-1}. Because the error bars are so large, the tension with SH0ES is remarkably small, at just under 1σ. When we add the SH0ES constraint, the precision of the fit improves considerably to $H_0 = 73.27 \pm 1.31$ km s^{-1} Mpc^{-1}, giving us a reduction in tension of 0.85σ. Both of these

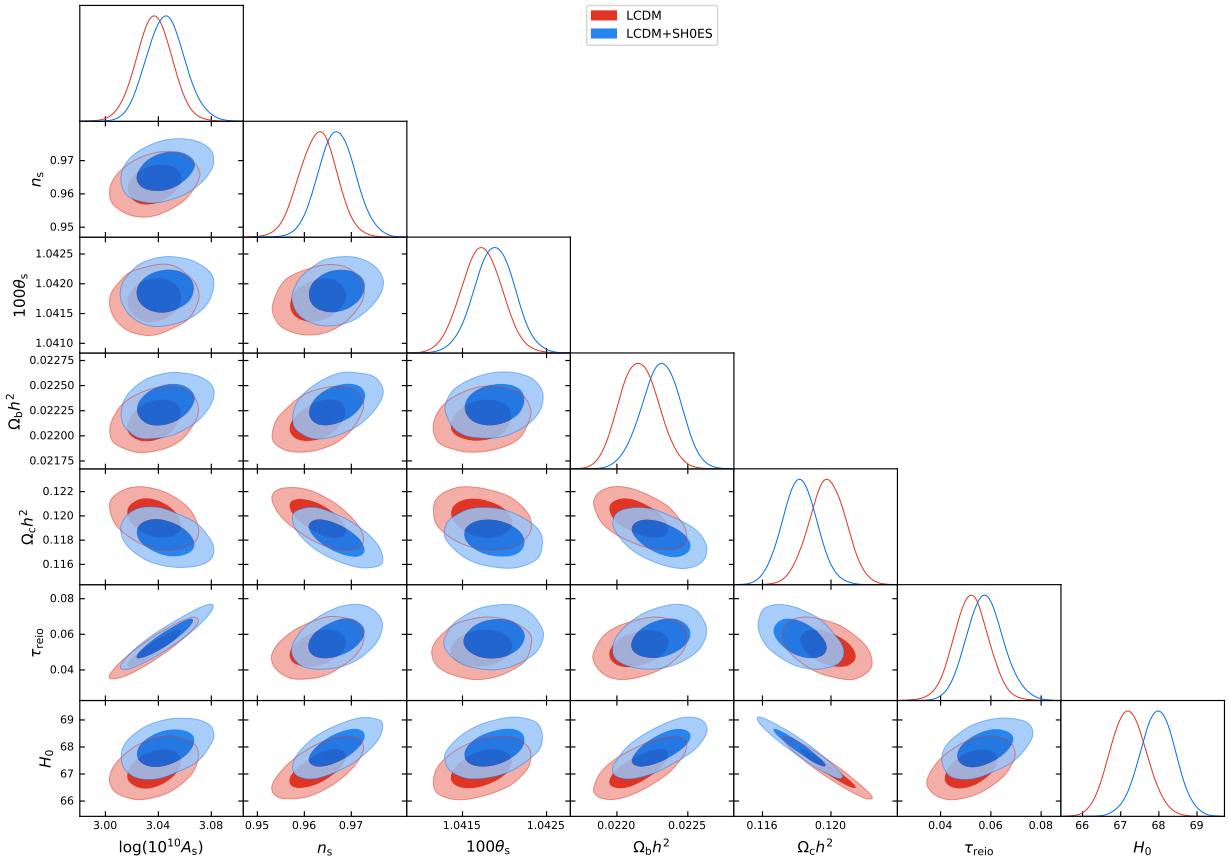

Figure 3.1 Corner plot showing both ΛCDM runs. The run without the SH0ES constraint is in red, and the run with the constraint is in blue. Distributions are clearly slightly different (for most parameters) with the constraint. We are of course most interested in the distributions for H_0, which can be found on the bottom row.

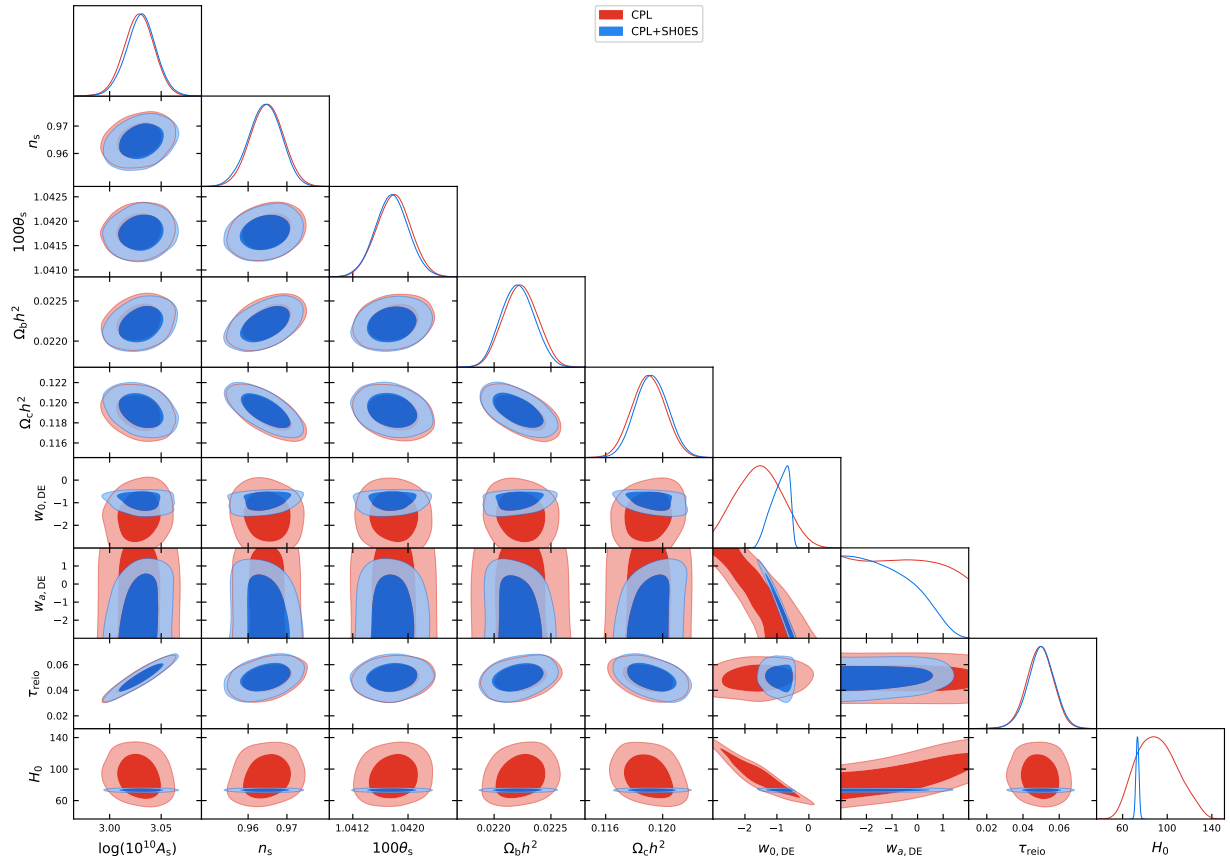

Figure 3.2 Corner plot showing both CPL runs. The run without the SH0ES constraint is in red, and the run with the constraint is in blue. Distributions are mostly unaffected by the addition of the constraint, except for the two model parameters (w_0 and w_a) and for H_0. We note that the scale provided for the H_0 distributions is much greater, relatively speaking, than the scale for the other parameters. This is due to the large error bars on H_0 in the CMB only run.

results are consistent with e.g. ref. [30]—which similarly finds that H_0 in CPL is almost entirely unconstrained by the CMB alone, but very tightly constrained when also constrained by SH0ES' H_0 value—so we are not concerned by the dramatic improvement.

A corner plot illustrating our results is given in figure 3.2. We note that the base parameter distributions are essentially unaffected by the addition of the SH0ES constraint; the posteriors are only significantly updated for the model parameters (w_0 and w_a) and for H_0.

3.3 EADE

In the EADE+CMB picture, we found $H_0 = 66.27 \pm 0.95$ km s^{-1} Mpc^{-1}. This is noticeably lower than the value found in ref. [14], and is in similar disagreement with SH0ES as ΛCDM is. Adding the SH0ES constraint betters the situation only slightly, bringing us up to $H_0 = 67.78 \pm 0.50$ km s^{-1} Mpc^{-1}, for a reduction in tension of 0.25σ. In contrast, ref. [14] found $H_0 = 70.06^{+1.13}_{-1.09}$ km s^{-1} Mpc^{-1}—much closer agreement with SH0ES.

A corner plot illustrating our results can be found in figure 3.3. As with ΛCDM, most parameters are noticeably affected by the addition of the SH0ES constraint. We note that the posteriors for the two model parameters appear to have been insufficiently explored; we will discuss this in more detail shortly.

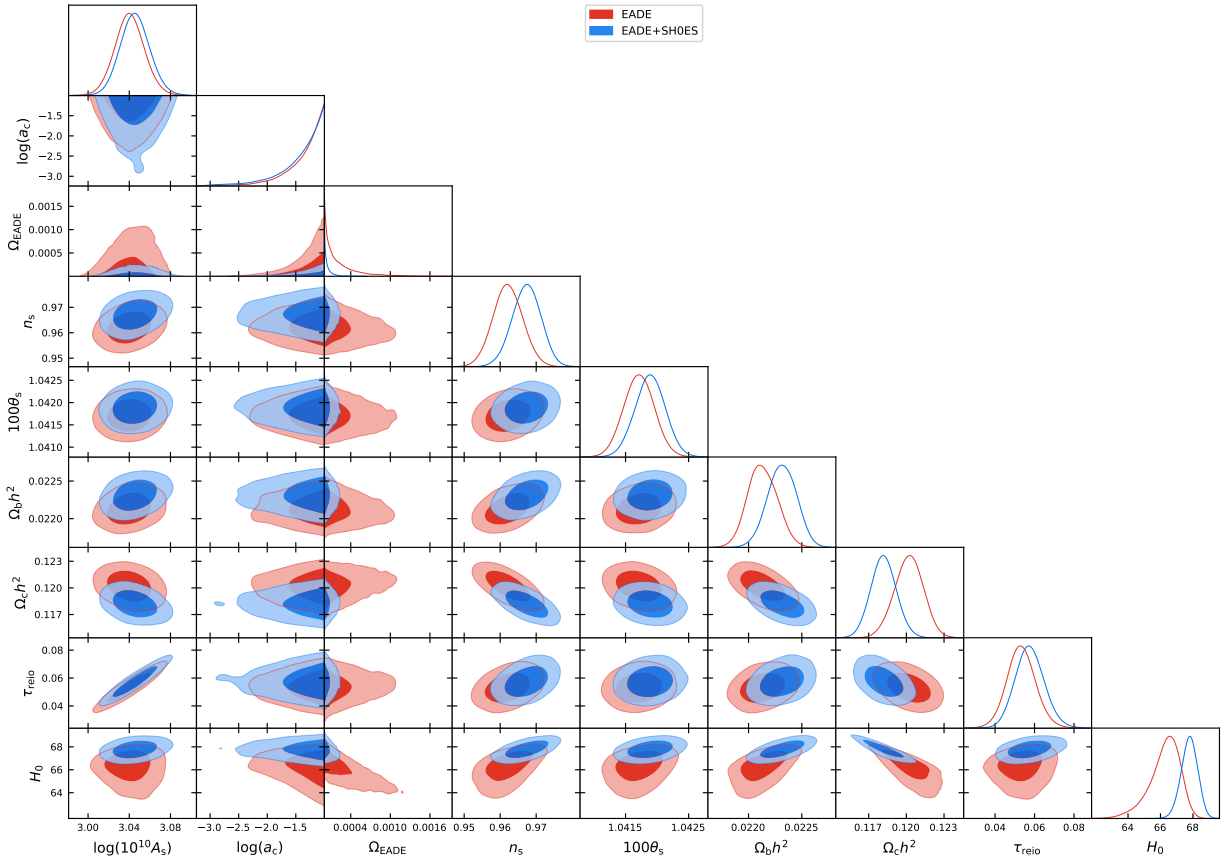

Figure 3.3 Corner plot showing both EADE runs. The run without the SH0ES constraint is in red, and the run with the constraint is in blue. We note that the posteriors for both $\log a_c$ and Ω_{EADE} seem to be insufficiently explored; we will discuss this more later. As with ΛCDM, adding the SH0ES constraint consistently shifts the H_0 distributions to higher values.

Chapter 4

Discussion and conclusion

Early universe measurements of H_0 most often use CMB data to constrain parameter values, with Planck being the most common choice of source for that data. However, extra constraints such as the SH0ES measurement of H_0 are also common. In this work, we have attempted to shed some light on the impact of this extra constraint on early universe measurements of H_0. We have done so by analyzing three different models—base ΛCDM, and two dynamical dark energy modifications of ΛCDM—using both Planck CMB data and a combination of Planck CMB data and the SH0ES measurement. We have followed the standard procedure for deriving H_0 values from the CMB, using the code `CLASS` to compute the CMB from proposed parameter values, and the code `Cobaya` to compare those computed values to real world data and generate distributions for each parameter.

In all cases, we found that the goodness-of-fit χ^2 parameter worsened with the addition of the SH0ES constraint. However, we do not believe that this indicates that adding a SH0ES constraint is a poor decision; rather, the addition of the SH0ES constraint also adds a degree of freedom to the χ^2 distribution, therefore producing a larger total χ^2.

Our value for H_0 in the ΛCDM+CMB case was 67.20 ± 0.48 km s^{-1} Mpc^{-1}; this agrees well with the value found by the Planck collaboration, showing that our overall pipeline is set up reasonably and there are no obvious errors with software installation or execution. If we compute

the statistical tension between our measurement and Planck's measurement in the usual way, we find a difference of 0.29σ, which is well within a standard deviation. At any rate, some minor variation from Planck's results is not entirely implausible, since we are using random sampling extensively in our analysis.

We found that further constraining ΛCDM with the SH0ES measurement of H_0 gave $H_0 = 67.97 \pm 0.46$ km s^{-1} Mpc^{-1}, producing a slight reduction in the tension with SH0ES of 0.64σ. Note that equation 1.4 can be made smaller either by reducing the difference between two measurements or by increasing the uncertainties on a measurement; since the uncertainties became smaller in this case, this reduction in tension can be attributed entirely to a shift in the central value.

H_0 is extremely poorly constrained by CPL+CMB: our measured value is $H_0 = 90.92 \pm 17.99$ km s^{-1} Mpc^{-1}. In this case, the central value agrees with neither Planck nor SH0ES, though the error bars are large enough to encompass both measurements. In fact, the uncertainty here is on the order of 20%. We note that this is consistent with previously published results for CPL dark energy; see for instance ref. [30]. More recent results for CPL with additional constraints from the Dark Energy Spectroscopic Instrument and other datasets are also generally in agreement with our results for w_0 and w_a [31].

Adding a constraint from SH0ES produces much better results: $H_0 = 73.27 \pm 1.31$ km s^{-1} Mpc^{-1}, in tension with SH0ES at only 0.14σ. This is once again in agreement with results from ref. [30]. However, given that the unconstrained measurement from CPL fully encompassed the SH0ES measurement, we have not learned very much from this result. The addition of the SH0ES constraint essentially selected the SH0ES H_0 from the initial wider range. This should not be entirely surprising, but it also does not provide much new information.

We should note some interesting features of our EADE results compared to the original paper [14]. They found $H_0 = 68.21^{+0.95}_{-2.72}$, with $\log a_c = -3.46^{+0.29}_{-0.22}$. In contrast, we found $H_0 = 66.27 \pm 0.95$, with $\log a_c = -1.35 \pm 0.33$. Qualitatively, this higher value for the critical scale factor implies

a later transition in the behavior of the EADE component, which apparently leads to a lower value for H_0. Further, we found $\Omega_{\text{EADE}} = 0.000234 \pm 0.000275$, corresponding to $f_c = 0.000711$ by way of equation 2.10; whereas ref. [14] found $f_c = 0.062^{+0.028}_{-0.031}$. We reemphasize that equation 2.10 has been problematic for us in the past, so we are unsure if this is a good comparison to be making; however, it is the only one we can easily make. These parameter comparisons are summarized in table 4.1.

Parameter	**CMB**	**CMB+SH0ES**
H_0	$68.21^{+0.95}_{-2.72}$ (66.27 ± 0.95)	$70.06^{+1.13}_{-1.09}$ (67.78 ± 0.50)
$\log a_c$	$-3.46^{+0.29}_{-0.22}$ (-1.35 ± 0.33)	$-3.46^{+0.28}_{-0.22}$ (-1.40 ± 0.39)
Ω_{EADE}	0.00267 (0.000234 ± 0.000275)	0.00272 $(0.0000503 \pm 0.0000622)$
f_c	$0.062^{+0.028}_{-0.031}$ (0.000711)	$0.063^{+0.027}_{-0.030}$ (0.000160)

Table 4.1 Best fit EADE parameter values from ref. [14] and this work; our values are given in parentheses. H_0 is reported in units of km s^{-1} Mpc^{-1}, and all other parameters are unitless. Our values for f_c and ref. [14]'s values for Ω_{EADE} are computed using equation 2.10. There are no clear connections between the two sets of values; notably, $\log a_c$, Ω_{EADE}, and f_c differ between our work and ref. [14] by at least an order of magnitude.

It is unclear if the differences between our results and those of ref. [14] are merely due to the use of different code, or something more significant. One potential cause stems from a numeric approximation called PPF that `CLASS` defaults to for models of this type; our assumption was that since PPF is the default approach in `CLASS` it would be acceptable to use here, but it is possible we were mistaken. That being said, this implementation difference cannot be the only issue, as it should not affect `Cobaya`'s ability to find a feasible initial point—and yet, when we otherwise

followed ref. [14]'s implementation, `Cobaya` could not find an initial point.

Not everything is in disagreement, however. The distribution for H_0, in the lower right corner, has a distinctly long lower tail. This same tail can be seen in the results of ref. [14], though it occurs at slightly different values. The distribution taking on a similar shape leads us to believe the different values could potentially be due to something more subtle in how `CLASS` works relative to `CAMB`.

We note that our posteriors for both $\log a_c$ and Ω_{EADE} are clearly not well explored. We attribute this at least partially to the relatively different parameter values we found. We based our prior distributions on the best fit values from ref. [14], which only overlap with our best fits in the tails. We also employed the same maximum and minimum values as ref. [14], but the maximum value in particular appears to be truncating our posterior distribution fairly significantly. Thus, another set of runs, with the priors centered more around the best fit values we found here and with a higher maximum value, is probably necessary before drawing any significant conclusions. We also note that given the relative scale of the Ω_{EADE} parameter, it would probably be wise to sample that parameter logarithmically, as with a_c.

As with ΛCDM, adding a SH0ES constraint does slightly alleviate the tension, going from 4.81σ to 4.56σ. However, this reduction is not as significant as that found by ref. [14]. Again, we are unsure exactly why this is, but some sort of difference between `CLASS` and `CAMB` seems most likely. Otherwise, the distributions for the two model parameters exhibit the same issues as in the unconstrained fit.

Broadly, we can see that adding a constraint on H_0 from SH0ES does generally decrease the Hubble tension. However, the causes for this decrease are not necessarily uniform: for ΛCDM and EADE, the predicted H_0 value shifted slightly; whereas for CPL, there was merely an increase in precision. Further, it is clear from figures 3.1 and 3.3 that in cases where H_0 is already well constrained by the CMB alone, adding a SH0ES constraint merely skews the predicted value slightly

higher, and never very far from the unconstrained value. It does not change the prediction very meaningfully.

Thus, we might conclude that it is most useful to add the SH0ES constraint in cases where H_0 is poorly constrained by the CMB alone, as with CPL. However, we argue that even in this case the addition of the constraint does not provide very much information: we start with a prediction so broad that it completely encompasses the SH0ES value, so adding the constraint serves only to select that specific value from the previous prediction. While this technically reduces the tension, we might as well look at the CMB only H_0 value and see that SH0ES is in good agreement with it and leave the matter there.

We therefore conclude that it is unclear what advantage adding the SH0ES constraint provides, at least on its own. In every case here, adding the constraint essentially told us exactly what we would expect, and did not add any new information. It is possible that employing this constraint in conjunction with data from e.g. baryon acoustic oscillations would be more informative.

We emphasize, however, that these results are probably not extensive enough to generalize to all extensions of ΛCDM. Conducting a similar analysis with even more cosmological models would be useful follow up work; it is possible that there are models where adding the constraint from SH0ES would provide meaningful information. Another interesting avenue for future research would be conducting this same analysis with different extra constraints and combinations of constraints. Other common constraint choices include baryon acoustic oscillations, supernova surveys, and large scale structure surveys [4]. It would be instructive to quantify the impact of these constraints as well, since they are also in common use.

Appendix A

SH0ES: distance ladder measurements

In this appendix we will outline the distance ladder measurement of H_0, paying specific attention to the methods used by the SH0ES collaboration. We note that there are many other late universe measurements, and even other distance ladder measurements. (See, for example, [32].)

At a very high level, the goal with distance ladder measurements of H_0 is to measure both distances to and recessional velocities of a large number of galaxies. Plotting recessional velocity versus distance shows a nice linear trend; fitting a line and taking the slope gives H_0 [33]. The most difficult element of this measurement is the distance measurements; the bulk of this appendix will explain how astronomers approach those.

A.1 Distance measurements

Until extremely recently, if astronomers wanted to study something in space, they needed to use light to do it. Now there are gravitational wave observatories and neutrino detectors, but both of those technologies are still relatively new. Thus, with few exceptions, anything we want to know about an object has to be able to be determined from the light we get from it. This includes distances.

When we observe a distant object and measure how bright it is, we are measuring a quantity

called flux. Flux has dimensions of power per area. Mathematically, it is defined thus:

$$F = \frac{L}{4\pi R_L^2}. \tag{A.1}$$

Here, F represents the flux and L denotes the intrinsic power output of the source, which is called luminosity. R_L is the "luminosity distance" from the observer to the source, which we treat here as the radius of a sphere centered on the source [33]. Thus, if we know one of flux or luminosity and can measure the other, we can use this equation to determine the distance. Typically, flux is what we measure, so we need to already know luminosity. This is where standard candles come in.

Standard candles are astronomical objects whose brightness is tied to some property that we can observe from very far away. For instance, one type of standard candle is a class of stars called Cepheid variables. These stars grow brighter and then dimmer with time, in a periodic manner. There is a convenient relationship between the length of a Cepheid's period and its average luminosity. Consequently, we only need measure a Cepheid's period—giving us its average luminosity—and its average flux, and we can compute a distance to the Cepheid [33]. The difficulty in this process arises from the need to calibrate such measurements: we have no intrinsic knowledge of the relationship between Cepheids' periods and luminosities.

This leaves us needing some sort of way to measure distances independent of an object's brightness. The usual approach is to use parallax. Parallax is a trigonometric technique that allows us to measure distances to celestial objects without knowing anything about how bright they are. The idea is to construct a triangle with the object you are observing at one vertex, and two observations that you make at the other vertices. You can measure the distance between your two observations, giving you the length of one side of the triangle. Because we perceive distant things as moving less than near things, we can measure the projected angular motion of e.g. a star against the background of further stars. Then, since we have an angle and a side length, we can determine another side length—the distance to the star [33]. Because this technique requires us to be able to resolve individual stars, we are limited in how far we can measure using it.

Parallax is the first step in what astronomers call the distance ladder. We can use parallax to measure distances to many Cepheids, giving us a way to calibrate Cepheids as a standard candle. Cepheids are not bright enough to measure distances to very many galaxies, so we can then use many Cepheid distance measurements to calibrate other standard candles—typically type Ia supernovae—and use those to measure distances to a large number of galaxies. This finally gives us enough data points to compute the Hubble constant [8, 33].

These three types of measurements—parallax, Cepheids, and supernovae—are the steps in the distance ladder employed by the SH0ES collaboration [8]. Other steps are possible, however. Parallax is usually the first step, but a common replacement for the Cepheid step is something called the Tip of the Red Giant Branch (TRGB). Stars of a certain mass and age will share the same brightness, so we can use a known class of star as a standard candle. This method employs one such class, which is easily identified due to a rapid transition when stars start burning helium. This rapid transition creates a distinct "tip" in parameter space [33]. One distance ladder measurement of H_0 made using TRGB distances can be found in [32]. As can be seen in that paper and in ref. [4], these TRGB measurements often fall between the CMB and Cepheid-based distance ladder measurements.

A.2 Velocity measurements

We still need to address how we obtain distance measurements for all of these galaxies we have measured distances to. The key element here is the Doppler equation, which for nearby objects looks like

$$v = \frac{\Delta\lambda}{\lambda_0} c. \tag{A.2}$$

Here c is the speed of light, λ_0 is some expected wavelength of light, and $\Delta\lambda$ is the difference between the wavelength we observe and what we expect. c is known, and it is relatively easy

to determine the wavelength of light we are receiving from a distant galaxy. Thus, if we could determine what wavelength of light the galaxy is emitting, we could calculate a velocity [33].

The primary tool astronomers use to overcome this difficulty is atomic spectra. Galaxies often have features in their spectra that are identifiable as being associated with some particular element; the true wavelengths of these features are known. So we can determine a galaxy's velocity by observing its spectrum and figuring out how much it is shifted by [33].

A.3 Summary

This is a very high level description of distance ladder measurements, but we feel it is sufficient for our purposes here. In reality, some of the analysis required can be very technical, especially for the distance ladder calibrations [8]. It is in these calibrations that most of the potential for error in the SH0ES measurement lies. However, since we are not focusing on the SH0ES measurement, we do not feel the need to explain in further depth.

Appendix B

Constraining cosmological models using the CMB

In this appendix we give a more conceptual overview of the Planck measurement of H_0. We especially focus on how the CMB can constrain cosmological parameters. We begin with a brief description of ΛCDM cosmology, and then focus on connecting that model's features to the CMB. This connection is what allows us to make parameter measurements from the CMB, and therefore what allows us to measure H_0 from the CMB.

B.1 ΛCDM

The main points of ΛCDM are summarized by the Planck collaboration [18] thus:

1. Physics is the same throughout the universe
2. General relativity is an adequate description of gravity
3. On large scales the universe is statistically the same everywhere

4. The universe was once much hotter and denser and has been expanding since early times
5. There are five cosmological constituents:
   (a) Dark energy which functions like vacuum energy
   (b) Pressureless dark matter which interacts with normal matter only gravitationally
   (c) Regular atomic matter
   (d) The CMB photons
   (e) Nearly massless neutrinos which are relativistic and non-interacting at the time of CMB formation
6. The curvature of space is very small
7. Density variations were set at early times and are Gaussian, adiabatic, and scale invariant—they are proportional in all constituents of the universe and have similar amplitudes as a function of scale
8. The observable universe has trivial topology

Several of these points may seem fairly obvious; for instance, general relativity is easily the best-tested theory of gravitation we have, so using anything else to describe gravity would not make much sense. Other points are not particularly relevant to our discussion: the topology of the universe has minimal effect on discussions of its expansion rate. We provide all of these points merely to give an accurate picture of where we start with ΛCDM, especially since many proposed solutions to the Hubble tension are cosmological models that modify one or more of these points. (For example, there are many models that tweak the model of gravitation slightly, but leave everything else the same.)

Many of these components of ΛCDM have one or more parameters that are associated with them: dark energy is strongly governed by its equation of state, the statistical distribution of matter

(often described with a power spectrum) is important to the formation of structure and curvature, the history of the universe's expansion is obviously related to the universe's expansion rate. These parameters are what allow us to more fully describe our cosmological model; without values for these parameters we would know for instance that the universe is expanding but not to what extent.

B.2 Constraints from the CMB

We have already provided a visualization of the CMB in figure 2.1. The CMB's formation is a complicated subject, but the key thing to know is that it formed when photons no longer consistently interacted with "normal" baryonic matter [2]. Until this time, which is known as the epoch of recombination, photons and baryons formed a homogeneous fluid. After the epoch of recombination, photons no longer consistently interacted with baryons, and were able to stream freely through the universe. These photons are what we see as the CMB; photons that were in a slight overdensity in the fluid at recombination will be slightly warmer and will show up as hot spots on the CMB, while similar effects apply for cooler photons [2].

The power spectrum of the temperature fluctuations (defined in eq. 2.4) can be seen in figure 2.2. This power spectrum can be roughly thought of as the magnitude of temperature deviations as a function of angular scale. Thus, both hot and cold spots might contribute to the same peak in the spectrum, if they occur on the same scale and are the same magnitude.

As outlined in chapter 2, this power spectrum is the primary thing being fit to when using MCMC methods to derive cosmological parameters from the CMB, as well as polarization power spectra. Thus, we should be able to connect various features in the power spectrum to the cosmological parameters we desire to constrain. In our case, these parameters are $\Omega_b h^2$, $\Omega_c h^2$, $100\theta_s$, τ, n_s, and $\ln\left(10^{10}A_s\right)$ [7]. The first two parameters are density fractions scaled by $h = H_0/100$ for normal matter and CDM respectively; we will explain $100\theta_s$ in a moment; τ is the optical depth of the

universe at an epoch called reionization; and the final two parameters are related to the distribution of matter throughout the universe. We note that none of these parameters are H_0; however, it is closely related to $100\theta_s$ [2]. While H_0 is also related to the two density parameters, those are also degenerate with the pure density fractions Ω_b and Ω_c, so $100\theta_s$ is usually used to constrain H_0 and then that value is used to help constrain the density fractions. Thus, we will focus on how the CMB power spectrum constrains $100\theta_s$, and we will not concern ourselves with the other parameters. We do note that brief explanations of how the other parameters are constrained by the CMB can be found in refs. [2, 34, 35].

First, let us discuss what $100\theta_s$ represents. An important concept in cosmology is that of horizon distances: a horizon distance is the farthest distance some signal could travel given its speed and how long it had to travel. The current horizon distance around the earth for light is about 14 billion light-years: since the universe is about 14 billion years old, light cannot have traveled any further than that. We can also discuss horizon distances for acoustic signals. The pre-CMB photon-baryon fluid was full of pressure waves; the furthest distance these waves could have traveled between the Big Bang and recombination is called the sound horizon distance, and is usually denoted d_s. θ_s is the angular projection of this distance onto the sky, and it is often scaled by a factor of 100 for computational purposes [2].

The sound horizon distance is primarily constrained by the first peak in the CMB temperature power spectrum. Prior to recombination, the photon-baryon fluid was primarily influenced by gravitational fields created by dark matter. Slight overdensities in the dark matter caused compression in the fluid; however, as the fluid compressed its pressure rose. This caused decompression, until the fluid became diffuse enough to lose pressure and start collapsing inward again. This cycle of standing waves continued until recombination [2].

At recombination, if a photon was in a compression, it would be slightly hotter than the average temperature of the CMB—vice versa for photons in decompressions. Photons at one extreme or the

other contribute to the first peak in the power spectrum. The distance scale associated with these fluctuations is the sound horizon distance; thus, the angular position of the first peak in the power spectrum should be similar to θ_s [2].

Now we must connect θ_s to H_0. We can relate angular scales to actual scales like

$$\theta_s = \frac{d_s}{d}, \tag{B.1}$$

where d is the distance to the thing whose scale we are concerned with. θ_s is constrained by the CMB of course, and d_s can be computed by determining the speed of sound in the photon-baryon fluid (about $c/\sqrt{3}$), since the amount of time prior to recombination is more or less known. Consequently, we can use this relationship to obtain d—the distance from us to the CMB. For a higher expansion rate, H_0, we would expect d to be larger; and for a lower H_0, we would expect it to be smaller. Thus, the angular position of the first peak constrains H_0 [2].

Computationally, this works by `CLASS` using a specified value for θ_s to infer the corresponding H_0 value. These values (for θ_s and H_0) are passed back to `Cobaya` which checks them against the Planck likelihood, which directly constrains θ_s, and the SH0ES likelihood, which directly constrains H_0.

We reiterate that all of the other parameters are similarly constrained by the CMB; however, we will not go into detail here. We also note that the precise physics constraining θ_s and H_0 are of course more technical than the description we have provided here; we merely hoped to give the reader a conceptual understanding of how the CMB can constrain cosmological parameters.

Bibliography

[1] A. Friedman, "Über die Krümmung des Raumes," Zeitschrift für Physik **10,** 377–386 (1922).

[2] B. Ryden, *Introduction to Cosmology*, 2nd ed. (Cambridge University Press, 2017).

[3] E. Hubble, "A relation between distance and radial velocity among extra-galactic nebulae," Proceedings of the National Academy of Sciences **15,** 168–173 (1929).

[4] E. D. Valentino, O. Mena, S. Pan, L. Visinelli, W. Yang, A. Melchiorri, D. F. Mota, A. G. Riess, and J. Silk, "In the realm of the Hubble tension—a review of solutions," Classical and Quantum Gravity **38,** 153001 (2021).

[5] A. G. Riess *et al.*, "Observational Evidence from Supernovae for an Accelerating Universe and a Cosmological Constant," The Astronomical Journal **116,** 1009–1038 (1998).

[6] J. P. Huchra, "The Hubble Constant,", https://lweb.cfa.harvard.edu/~dfabricant/huchra/hubble/, 2008, [Accessed May 12, 2025].

[7] Planck Collaboration VI, "Planck 2018 results. VI. Cosmological parameters," (2018).

[8] A. G. Riess *et al.*, "A Comprehensive Measurement of the Local Value of the Hubble Constant with 1 km s^{-1}Mpc^{-1} Uncertainty from the Hubble Space Telescope and the SH0ES Team," The Astrophysical Journal Letters **934,** L7 (2022).

[9] J. Silk, "Towards the Limits of Cosmology," Foundations of Physics **48,** 1305–1332 (2018).

[10] D. S. Lemons, *An Introduction to Stochastic Processes in Physics* (The Johns Hopkins University Press, 2002), p. 34.

[11] N. Christensen, R. Meyer, L. Knox, and B. Luey, "Bayesian methods for cosmological parameter estimation from cosmic microwave background measurements," Classical and Quantum Gravity **18,** 2677 (2001).

[12] M. CHEVALLIER and D. POLARSKI, "ACCELERATING UNIVERSES WITH SCALING DARK MATTER," International Journal of Modern Physics D **10,** 213–223 (2001).

[13] E. V. Linder, "Exploring the Expansion History of the Universe," Physical Review Letters **90,** 091301 (2003).

[14] L. Yin, "Reducing the H_0 tension with exponential acoustic dark energy," The European Physical Journal C 82 (2022).

[15] Planck Collaboration *et al.*, "Planck 2013 results. XII. Diffuse component separation," A&A **571,** A12 (2014).

[16] ESA, "Planck's power spectrum of temperature fluctuations in the Cosmic Microwave Background,", https://sci.esa.int/web/planck/-/51555-planck-power-spectrum-of-temperature-fluctuations-in-the-cosmic-microwave-background, 2013, [Accessed May 17, 2025].

[17] C. L. Bennett *et al.*, "Scientific results from the Cosmic Background Explorer (COBE) (microwave/infrared) Introduction to the COBEII and Mission Objectives,", 1993.

[18] Planck Collaboration I, "Planck 2018 results - I. Overview and the cosmological legacy of Planck," A&A **641,** A1 (2020).

[19] D. Blas, J. Lesgourgues, and T. Tram, "The Cosmic Linear Anisotropy Solving System (CLASS). Part II: Approximation schemes," Journal of Cosmology and Astroparticle Physics **2011,** 034–034 (2011).

[20] J. Torrado and A. Lewis, "Cobaya: code for Bayesian analysis of hierarchical physical models," Journal of Cosmology and Astroparticle Physics **2021,** 057 (2021).

[21] J. Torrado and A. Lewis, "Cobaya: Bayesian analysis in cosmology,", Astrophysics Source Code Library, record ascl:1910.019, 2019.

[22] A. G. Riess, S. Casertano, W. Yuan, J. B. Bowers, L. Macri, J. C. Zinn, and D. Scolnic, "Cosmic Distances Calibrated to 1% Precision with Gaia EDR3 Parallaxes and Hubble Space Telescope Photometry of 75 Milky Way Cepheids Confirm Tension with LambdaCDM," (2020).

[23] N. Aghanim *et al.*, "Planck 2018 results. V. CMB power spectra and likelihoods," Astron. Astrophys. **641,** A5 (2020).

[24] A. Lewis and S. Bridle, "Cosmological parameters from CMB and other data: A Monte Carlo approach," Phys. Rev. **D66,** 103511 (2002).

[25] A. Lewis, "Efficient sampling of fast and slow cosmological parameters," Phys. Rev. **D87,** 103529 (2013).

[26] R. M. Neal, "Taking Bigger Metropolis Steps by Dragging Fast Variables," ArXiv Mathematics e-prints (2005).

[27] A. Lewis, "GetDist: a Python package for analysing Monte Carlo samples," (2019).

[28] A. Lewis, A. Challinor, and A. Lasenby, "Efficient computation of CMB anisotropies in closed FRW models," **538,** 473–476 (2000).

[29] C. Howlett, A. Lewis, A. Hall, and A. Challinor, "CMB power spectrum parameter degeneracies in the era of precision cosmology," **1204,** 027 (2012).

[30] W. Yang, E. D. Valentino, S. Pan, Y. Wu, and J. Lu, "Dynamical dark energy after Planck CMB final release and H0 tension," Monthly Notices of the Royal Astronomical Society **501,** 5845–5858 (2021).

[31] D. Collaboration *et al.*, "DESI DR2 Results II: Measurements of Baryon Acoustic Oscillations and Cosmological Constraints," (2025).

[32] W. L. Freedman, B. F. Madore, I. S. Jang, T. J. Hoyt, A. J. Lee, and K. A. Owens, "Status Report on the Chicago-Carnegie Hubble Program (CCHP): Three Independent Astrophysical Determinations of the Hubble Constant Using the James Webb Space Telescope," (2024).

[33] B. W. Carroll and D. A. Ostlie, *An Introduction to Modern Astrophysics*, 2nd ed. (Cambridge University Press, 2017).

[34] W. Hu, "Ringing in the New Cosmology,", https://background.uchicago.edu/~whu/intermediate/intermediate.html, [Accessed April 15, 2025].

[35] NASA, "Optical Depth to Reionization, τ,", https://lambda.gsfc.nasa.gov/education/graphic_history/taureionzation.html, [Accessed April 15, 2025].

Index